Pressure-induced structural and electronic transitions in InTeI

Xiaomeng Wang, Tong Chen, Beatriz H. Cogollo-Olivo, Chi Ding, Tianheng Huang, Qing Lu, and Jian Sun*

National Laboratory of Solid State Microstructures, School of Physics and Collaborative Innovation Center of Advanced Microstructures, Nanjing University, Nanjing 210093, China

(Received 5 February 2021; revised 25 July 2021; accepted 27 July 2021; published 9 August 2021)

Based on crystal structural search and *ab initio* calculations, we report pressure-induced structural and electronic phase transitions for the semiconductor indium tellurium iodine (InTeI). We have found two structures belonging to the same space group of InTeI at high pressure (labeled as $P4/nmm$-I and $P4/nmm$-II, respectively), where $P4/nmm$-II is metastable. Our calculation results show that the ambient $P2_1/c$ phase transforms to a tetragonal $P4/nmm$-I phase at about 15 GPa, characterized by the appearance of metallization and superconductivity with T_c of around 7 K. Besides, band-structure calculations suggest that the InTeI system undergoes a pressure-induced electronic phase transition from a direct to indirect band gap in the $P2_1/c$ phase. On the application of atomic substitution, the superconducting temperature T_c of InTeI can be further raised to around 9.7 K if the iodine atoms are replaced by the lighter chlorine atoms in the $P4/nmm$-I phase. The results pave the way for applying of Indium tellurohalide in optoelectronic devices and demonstrate a method that adjusts electronic properties by pressure or atomic substitution.

DOI: 10.1103/PhysRevB.104.064104

I. INTRODUCTION

Layered polar compound BiTeI has attracted a great deal of scientific attention and interest as a potential spintronic material due to several intriguing discoveries, including a giant Rashba-type spin splitting [1] and a pressure-induced topological insulating phase [2,3]. Subsequently, the experimental observation of infrared and Raman spectra revealed a structural phase transition at 9 GPa, possibly inhibiting the predicted topological high-pressure phase [4]. Meanwhile, a theoretical study predicted two high-pressure structural phase transitions ($P3m1 \rightarrow Pnma \rightarrow P4/nmm$) in BiTeI [5]. In other recent studies, Rusinov *et al.* studied both the topological and crystal phase transitions in the bismuth tellurohalides (BiTeX, X = I, Br, Cl) through density-functional calculations [6]. Qi *et al.* reported the discovery of superconductivity in both BiTeI and BiTeBr induced by pressure, while the resistivity at higher temperatures still exhibits semiconducting behavior [7]. Additionally, a few studies on the crystal and electronic structure of AuTeI and PdTeI have been reported [8]. These exciting discoveries have motivated us to explore the other metal tellurohalides, which may be an appealing candidate for numerous practical applications, such as optoelectronic materials [9,10], and quantum computing due to the coexistence of topological states and superconductivity [7,11–15]. By exploring crystal structures from the Database Materials Project [16], we discovered a layered wide-gap semiconductor InTeI with $P2_1/c$ symmetry, which was successfully synthesized in the 1980s [17]. Theoretically, 2D monolayer InTeI is predicted to be a promising optoelectronic material due to its tunable electronic properties and highly anisotropic carrier mobility [18].

It is well known that pressure is often an effective and clean way of modifying a compound's electronic structure to cause a phase transition, and sometimes it plays a critical role in the emergence of superconductivity. Recently, pressure-induced superconductivity was reported in bismuth iodide (BiI), in which bulk superconductivity appears only in the high-pressure phases [19]. Simultaneously, recent theoretical and experimental studies showed that substitution is a feasible method for tuning electronic properties [20–22]. For example, in the halogen hydrogen system, the superconductivity temperature (T_c) can be enhanced by substituting the halogen atoms. For instance, the T_c of $HCl_{0.5}Br_{0.5}$ at 170 GPa was predicted to be around 95 K, which is the highest record among all the known hydrogen halides so far [23]. Consequently, it is highly desirable to search for new structural phases of InTeI under high pressure, investigate the origin of possible superconductivity, and explore the effects of substituting other atoms.

In this work, combining crystal structure prediction techniques and first-principles calculations up to 40 GPa, we find a high-pressure phase (labeled as $P4/nmm$-I) and a metastable phase (labeled as $P4/nmm$-II), with their differences mainly in the arrangement of Te atoms. The structural calculations reveal that InTeI undergoes a structural phase transition: $P2_1/c \rightarrow P4/nmm$-I. The electronic structure, phonon spectrum, and electron-phonon (e-ph) coupling are investigated for these phases. Band-structure calculation of $P2_1/c$ phase reveals a direct to indirect electronic band-gap transition under pressure, and the critical turning pressure occurs at a range of 5–8 GPa. We find that the metastable phase $P4/nmm$-II is a topological metal with nontrivial surface states. Both $P4/nmm$-I and $P4/nmm$-II phases have relatively strong e-ph coupling. For the $P4/nmm$-I phase of InTeI, we also replace the iodine atoms with some lighter halogen atoms. Newly substituted compounds such as InTeBr and InTeCl are both

*jiansun@nju.edu.cn

 ©2021 American Physical Society

thermodynamically and dynamically stable, and they possess a higher T_c. $P4/nmm$-II of InTeI represents an example of a material with both superconductivity and topologically nontrivial surface states under high pressure. Finally, we plot a complete phase diagram with the single material of InTeI. Our results open up a direction for modulating band-gap and optical properties and illustrate that the substitution of light atoms plays an essential role in enhancing the superconductivity mediated by electron-phonon coupling.

II. COMPUTATIONAL METHODS

We performed a high-pressure crystal structures searching of InTeI using an in-house package called MAGUS (machine learning and graph theory assisted universal structure searcher) [24,25], in which we employed the Bayesian optimization [26] and graph theory to improve the search efficiency. This method has been applied successfully in many systems, such as helium compounds [27] and layered materials [28]. The maximum number of atoms in the simulation cell is no more than 24 atoms. The structural optimization and electronic structure calculations were carried out within density-functional theory (DFT) using the projector augmented-wave [29] method as implemented in the Vienna *Ab initio* Simulation Package (VASP) [30]. For the exchange-correlation functional, we choose the generalized gradient approximation (GGA) with the Perdew-Burke-Ernzerhof (PBE) formalism [31]. The valence electrons of the pseudopotentials are $4d^{10}5s^25p^1$ for In, $5s^25p^4$ for Te, and $5s^25p^5$ for I. The plane-wave energy cutoff was set as 400 eV, and the Brillouin zone was meshed using the Monkhorst-Pack method with a spacing of $2\pi \times 0.025$ Å^{-1} (the equivalent grid for $P2_1/c$, $P4/nmm$-I and $P4/nmm$-II phase at the highest pressure are $9 \times 12 \times 10$, $19 \times 19 \times 6$, and $16 \times 16 \times 8$, respectively). The van der Waals (vdW) interaction was taken into account through an additional calculation based on the DFT-D3 method [32,33]. In our atomic optimization, the tolerance in the atomic force was set to 0.001 eV/Å. Additionally, since the PBE exchange-correlation may underestimate band gap, the accurate hybrid functional HSE06 [34] was used to check the band structures of the $P2_1/c$ phase. The $2 \times 2 \times 2$ supercells were adopted to calculate the phonon dispersions of $P4/nmm$-I and $P4/nmm$-II structures using the finite-displacement method with the PHONOPY [35] code. The surface states were obtained by constructing the maximally localized Wannier functions [36] and using the surface Green function approach [37], as implemented in the WANNIERTOOLS package [38]. Electron-phonon coupling properties were calculated using density-functional perturbation theory, as implemented in the QUANTUM ESPRESSO code [39]. We adopted $18 \times 18 \times 6$ and $15 \times 15 \times 10$ k-point mesh for charge self-consistent calculation; $36 \times 36 \times 12$ and $30 \times 30 \times 20$ k-point mesh for e-ph linewidth integration; and $6 \times 6 \times 2$ and $3 \times 3 \times 2$ q-point mesh for the dynamical matrix of $P4/nmm$-I and $P4/nmm$-II structures, respectively.

III. CRYSTAL STRUCTURE UNDER HIGH PRESSURE

InTeI crystallizes in a monoclinic crystal structure with space group $P2_1/c$ (No. 14, $Z = 4$) under ambient conditions. $P2_1/c$ phase is a layered structure along with its crystal graphic a axis with atoms forming corrugated layers parallel to the bc plane. As there are few studies on the structural properties of InTeI under high hydrostatic pressure, we employed a machine-learning accelerated first-principles crystal structure prediction method on InTeI under pressure up to 40 GPa. We found an energetically preferable high-pressure phase: the tetragonal phase $P4/nmm$-I (No. 129, $Z = 2$) and a metastable phase $P4/nmm$-II (No. 129, $Z = 2$). There are some differences between these two phases, mainly in the arrangement of Te atoms. In $P4/nmm$-I phase, Te-In-I-I-In-Te sequence along the c axis forms atomic stacking. In $P4/nmm$-II phase, the square net formed by Te atoms is located on the ab plane, and the In and I atoms form unique zigzag In-I ladders, which are sandwiched between the Te square nets. The structures proposed in this study are illustrated in Figs. 1(a)–1(c), and the optimized lattice parameters of the two phases are summarized in Table I.

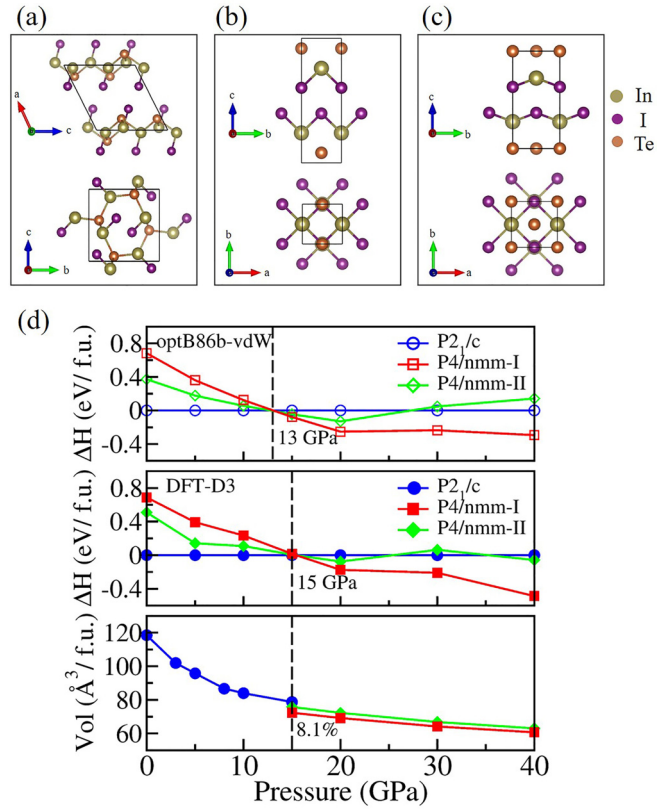

FIG. 1. Crystal structures of the three phases of InTeI and their enthalpy-pressure relations, and volume-pressure relations. (a)–(c) The crystal structures of the monoclinic $P2_1/c$ phase; the tetragonal $P4/nmm$-I phase; and the tetragonal $P4/nmm$-II phase, respectively; large brown and small purple and orange spheres denote In, I, and Te atoms, respectively. (d) The calculated enthalpy difference relative to the $P2_1/c$ phase using various exchange-correlation functionals and formula-unit volumes as functions of pressure. Theoretical calculations predict a structural phase transitions under high pressure, from $P2_1/c$ to $P4/nmm$-I at 15 GPa.

Because the ambient phase $P2_1/c$-InTeI is a layer stacked structure, we consider the van der Waals interaction for structure optimization. Table II presents the optimized lattice constants at 0 GPa with various vdW functionals [40]. Our

TABLE I. Calculated lattice parameters, atomic coordinates, and equivalent isotropic displacement parameters of the $P4/nmm$-I and $P4/nmm$-II phases of InTeI under high pressure (the atomic coordinates refer to the ITA-setting, and the transformation matrix from standard setting to the ITA-setting is (**P**,p):**a,b,c**;-1/4,1/4,0).

Phase	Lattice	Wyckoff positions				
(pressure)	parameters (Å)			x	y	z
$P4/nmm$-I	$a = 3.541$	Te	($2c$)	0.00000	0.50000	0.08088
(20 GPa)	$c = 11.029$	I	($2c$)	0.00000	0.50000	0.39703
		In	($2c$)	0.50000	0.00000	0.24031
$P4/nmm$-II	$a = 4.121$	Te	($2a$)	0.00000	0.00000	0.00000
(20 GPa)	$c = 8.527$	I	($2c$)	0.50000	0.00000	0.63283
		In	($2c$)	0.50000	0.00000	0.27623

results verified that the relative error of the lattice parameter is larger than those reported experimentally [17] when the normal GGA-PBE [31], vdW-DF [41], and vdW-DF2 [42] functionals were used. The calculated lattice constant a using GGA-PBE has a ∼12% error, although b and c have errors smaller than 2%. On the other hand, the errors of vdW-DF and vdW-DF2 are more consistent between a, b, and c, but their values are significantly larger with respect to the experimental ones. The structure parameters obtained with optB86b-vdW [43] and DFT-D3 [32,33] are within a 1% error bar compared to the experimental values.

We calculated the enthalpy-pressure (ΔH-P) curves [see Fig. 1(d)] with different functionals, including optB86b-vdW and DFT-D3, where the enthalpy differences ΔH are calculated with respect to the $P2_1/c$ structure. With the increase of pressure, InTeI undergoes a structural phase transition, and the transition pressure obtained with optB86b-vdW tends to shift to the lower pressure. As far as the DFT-D3 functional is concerned, InTeI transforms from the thermodynamic ground-state $P2_1/c$ structure to the $P4/nmm$-I structure at about 15 GPa. In all subsequent calculations, the DFT-D3 functional is employed in all phases of InTeI. The calculated volume-pressure (V-P) curves show that this phase transition can be characterized by first orders accompanying with 8.1% volume collapse at the critical pressure. Except for the energetics, the resulting phonon band structures without imaginary frequency prove the dynamical stability of the two structures.

We further consider the effects of finite temperature on the Gibbs free energies to investigate its structural stability at relevant simultaneous high P-T conditions. Our calculations are based on the quasiharmonic approximation (QHA) as implemented in the PHONOPY code [35].Our analysis is restricted here to temperatures below 5000 K. The P-T phase diagram is presented in Fig. 2. More interestingly, the phase boundary shows two remarkable features. First, the pressure location for the $P2_1/c$ to $P4/nmm$-I phase boundary is shifted towards lower pressures as the temperature rises. Second, we observe that the temperature phase transition boundary between the phases $P2_1/c$ and $P4/nmm$-I remains unchanged from 5 to 10 GPa as pressure increases. In order to confirm whether this feature is an artifact of the method or a physical characteristic, we perform the calculations with another functional, optB86b-vdW, in the range of 3–10 GPa. The results show that, unlike the previous cases, the shifts seen in the case of the $P2_1/c$-to-$P4/nmm$-I present no abnormal changes using optB86b-vdW functional. Therefore, our QHA results can be influenced by the selection of functional.

TABLE II. Calculated lattice parameters of InTeI at 0 GPa with different exchange-correlation functionals. The values in brackets are errors compared with the experimental values. The normal GGA-PBE, vdW-DF, and vdW-DF2 functionals give quite large errors, while the optB86b-vdW and DFT-D3 methods give better results.

	a (Å)	b (Å)	c (Å)	β (°)
Expt.	8.076	7.731	8.407	117.03
PBE	9.029	7.861	8.568	116.90
	(11.80%)	(1.68%)	(1.91%)	(−0.11%)
DFT-D2	7.569	7.966	7.893	114.88
	(−6.28%)	(3.04%)	(−6.11%)	(−1.84%)
DFT-D3	8.058	7.782	8.518	117.28
	(−0.22%)	(0.66%)	(1.32%)	(0.21%)
DFT-D3-BJ	7.888	7.704	8.467	117.31
	(−2.33%)	(−0.35%)	(0.71%)	(0.24%)
optB86b-vdW	7.937	7.754	8.487	117.22
	(−1.72%)	(0.30%)	(0.95%)	(0.16%)
optB88-vdW	7.994	7.809	8.561	117.41
	(−1.02%)	(1.01%)	(1.83%)	(0.32%)
optPBE-vdW	8.277	7.879	8.590	117.37
	(2.49%)	(1.91%)	(2.18%)	(0.29%)
vdW-DF	8.634	8.012	8.717	117.44
	(6.91%)	(3.63%)	(3.69%)	(0.35%)
vdW-DF2	8.420	8.064	8.860	117.95
	(4.26%)	(4.31%)	(5.39%)	(0.79%)

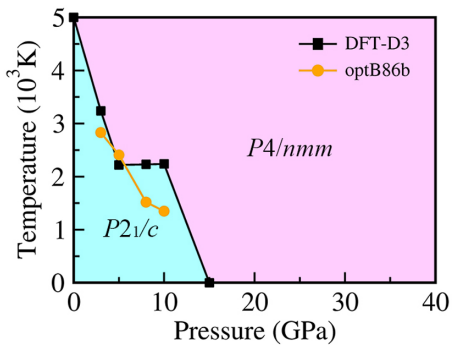

FIG. 2. Proposed finite-temperature phase diagram for InTeI.

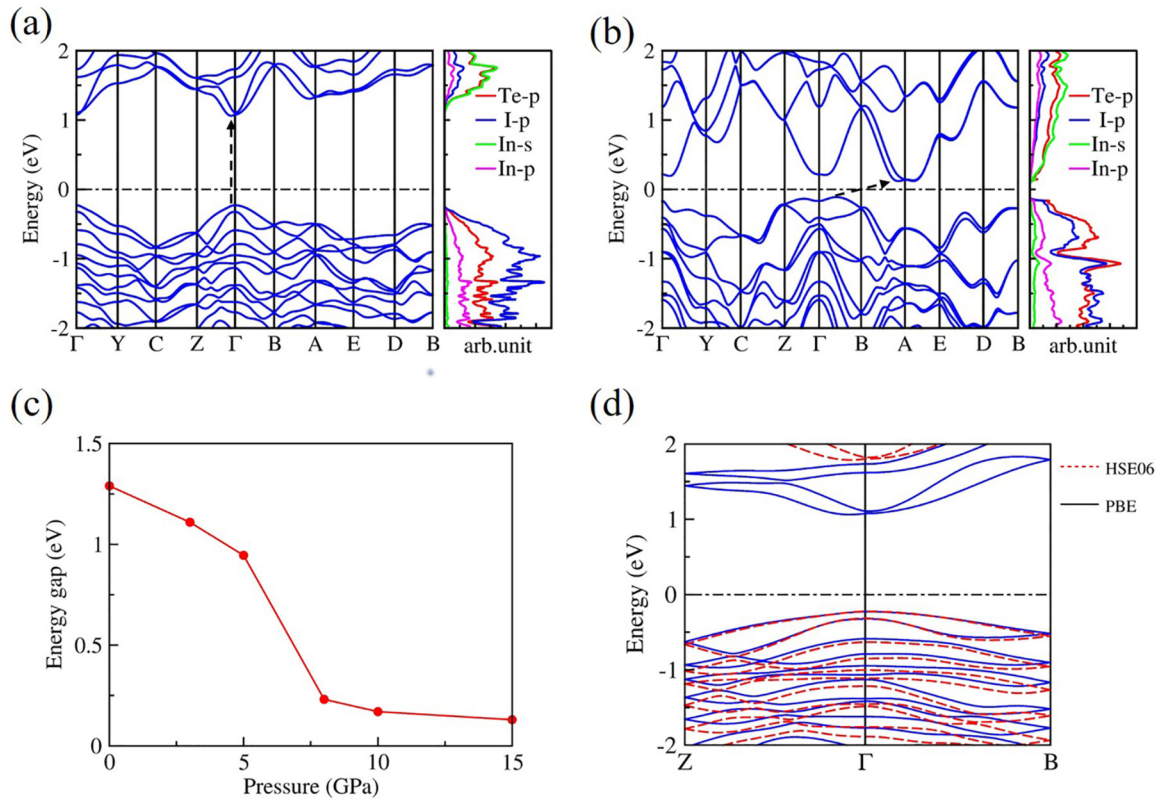

FIG. 3. Calculated electronic band structures and projected density of states of the $P2_1/c$ phase at 0 GPa (a) and 8 GPa (b) with SOC. (c)The size of the band gap versus pressure. (d) Band structures of the $P2_1/c$ phase at 0 GPa by the HSE06 method.

IV. ELECTRONIC PROPERTIES OF $P2_1/c$-INTEI UNDER PRESSURE

Our calculations reveal that the $P2_1/c$ phase of InTeI can exist only in a small pressure range. Within this stable pressure interval, we have calculated the electronic band structure of the $P2_1/c$ phase and examined the variation of the electronic band gap with pressure. The electronic band structures with the inclusion of spin-orbit coupling (SOC) at 0 GPa and 8 GPa are plotted in Fig. 3(a) and 3(b), respectively. The calculations show that InTeI at ambient pressure is a semiconductor with a direct bandgap of 1.29 eV. Both the conduction-band minimum (CBM) and the valence-band maximum (VBM) are slightly shifted towards the Γ point. As the applied pressure increases, the Γ and *A* valley of the conduction band go downward. For pressure around 8 GPa, the energy position of state at the conduction-band *A* valley becomes lower than that at the Γ valley, and the top of the valence band at Γ point develops a "Mexican-hat shaped" dispersion, as shown in Fig. 3(b), which results in an indirect band gap. In Fig. 3(c), we show the relationship between band-gap evolution versus pressure, where it can be seen how the band gap decreases, remaining quasidirect as the pressure increases. At 5 GPa, the gap drops dramatically to 0.23 eV, suggesting that InTeI may undergo an electronic phase transition. Besides, the band gap based on the HSE06 method is 2.01 eV, which is about 1 eV higher than that of PBE results, as shown in Fig. 3(d).

The analysis of the density of states (DOS) at 0 and 8 GPa [Figs. 3(a) and 3(b), respectively] show that the states at the CBM are mainly composed of In-*s* and Te-*p* character, while those at the VBM are mainly Te-*p* and I-*p* character derived. In order to understand the mechanism of the pressure-induced electronic phase transition from direct to indirect band gap, we carried out calculations of the bond parameters and the angle parameter under pressure, as shown in Figs. 4(a)–4(d). On the one hand, the In–Te bond lengths are shortened, and the internal θ angle of the In–Te–In bond is anomaly enlarged about 3° when the lattice is compressed to 8 GPa, resulting in a stronger coupling of the Te-*p* and In-*s* orbitals. Consequently, the band energy of the pair of states at CBM-Γ and CBM-*A* move towards the Fermi level, which leads to a sharp decrease of band gap at 5 GPa, as seen in Fig. 3(c). On the other hand, the coupling effect between the layers is also significant for the three crucial states mentioned above. Since the distance between layers changes significantly under pressure, the bands at CBM-Γ, CBM-*A*, and VBM-Γ are split, accelerating the reduction of the band gap. The isosurfaces of band-decomposed charge densities are also calculated. At different pressures for the phase $P2_1/c$, we selected points Γ and *A* at the CBM, and point Γ at the VBM. The results are presented in Figs. 4(e) and 4(f) for 0 and 8 GPa, respectively. It can be seen in the band-decomposed charge-density plots where the CBM-Γ, CBM-*A*, and VBM-Γ distributions gradually diffuse at high pressure. Therefore, with the increase of pressure, the out-of-plane orbitals begin to interact strongly, causing the shift in the position of the VBM. Additionally, the energy position of state at the CBM-Γ and CBM-*A* decrease until the CBM at the Γ point crosses over to the *A* point. This may be the reason that the band gap of InTeI changes from direct to indirect.

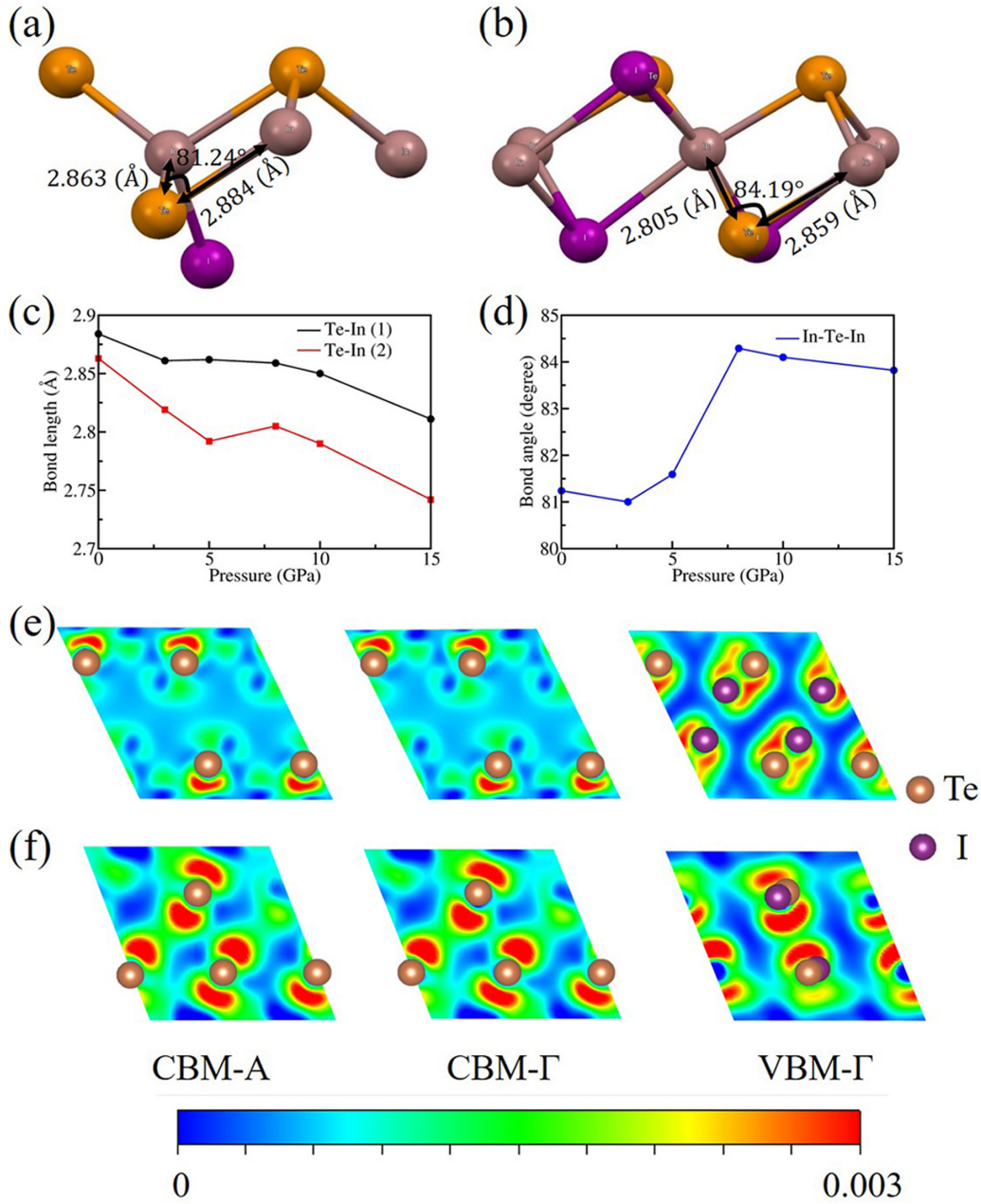

FIG. 4. The illustrations of InTeI (a) at 0 GPa and (b) at 8 GPa, respectively. The calculated (c) bond length of Te–In and (d) bond angle of In–Te–In as a function of pressure. Isosurfaces of the band-decomposed charge density for CBM-A, CBM-Γ, and VBM-Γ (e) at 0 GPa, and (f) at 8 GPa, respectively.

V. ELECTRONIC PROPERTIES OF HIGH-PRESSURE PHASE AND TOPOLOGICAL SURFACE STATES

To understand the electronic properties of the predicted high-pressure phase of InTeI, we calculated the electronic band structure and partial density of states (PDOS). Figures 5(a) and 6(a) display the band structure of $P4/nmm$-I and $P4/nmm$-II, respectively, indicating that both phases are metallic when SOC is omitted. It can be concluded that the change from a semiconductive behavior of the low-pressure phase to the metallic behavior of the high-pressure phase is concomitant with the structural transitions. We also calculated the band structure of $P4/nmm$-I and $P4/nmm$-II with SOC, respectively, as shown in Figs. 5(b) and 6(b). The results show that the $P4/nmm$-I phase of InTeI seems to be a trivial metal, while the $P4/nmm$-II phase exhibits unique electronic properties.

Then we focus on the electronic band structure of the $P4/nmm$-II phase of InTeI. Previous studies about $P4/nmm$–ZrSiS showed that the Si square net plays an essential role regarding the presence of Dirac feature [44], which matches the prediction by Young and Kane that new types of 2D Dirac semimetal can exist in 2D square lattices based on nonsymmorphic symmetry [45]. As a result, a line of Dirac nodes should also be expected in $P4/nmm$–II phase.

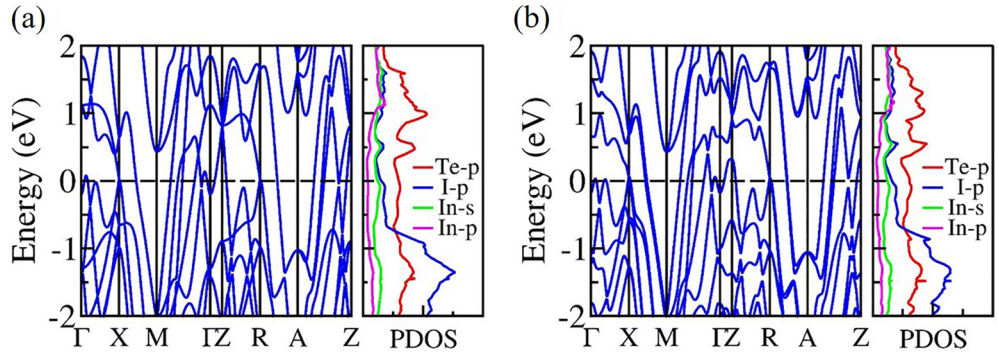

FIG. 5. Calculated electronic band structures and projected density of states of the $P4/nmm$-I phase at 20 GPa (a) without SOC and (b) with SOC.

From the projected band structure and PDOS [Figs. 6(a) and 6(b)], it shows that p orbitals of Te and I atoms, and the s orbitals of In atoms, mostly dominate the electronic states near the Fermi level. In the absence of SOC, several Dirac cones protected by the C_{2v} symmetry can be identified around the Fermi level E_F as indicated by violet circles. These Dirac cones form a line of Dirac nodes, resulting in a diamond-shaped Fermi surface [see Fig. 6(c)], which is very similar to the Fermi surface observed in the ZrSiS and related materials [44].

Due to the presence of the heavy atoms, the effect of SOC near the E_F cannot be neglected. As shown in Fig. 6(b), after considering the SOC effects in the band-structure calculations, the cones along the high-symmetry line gapped,

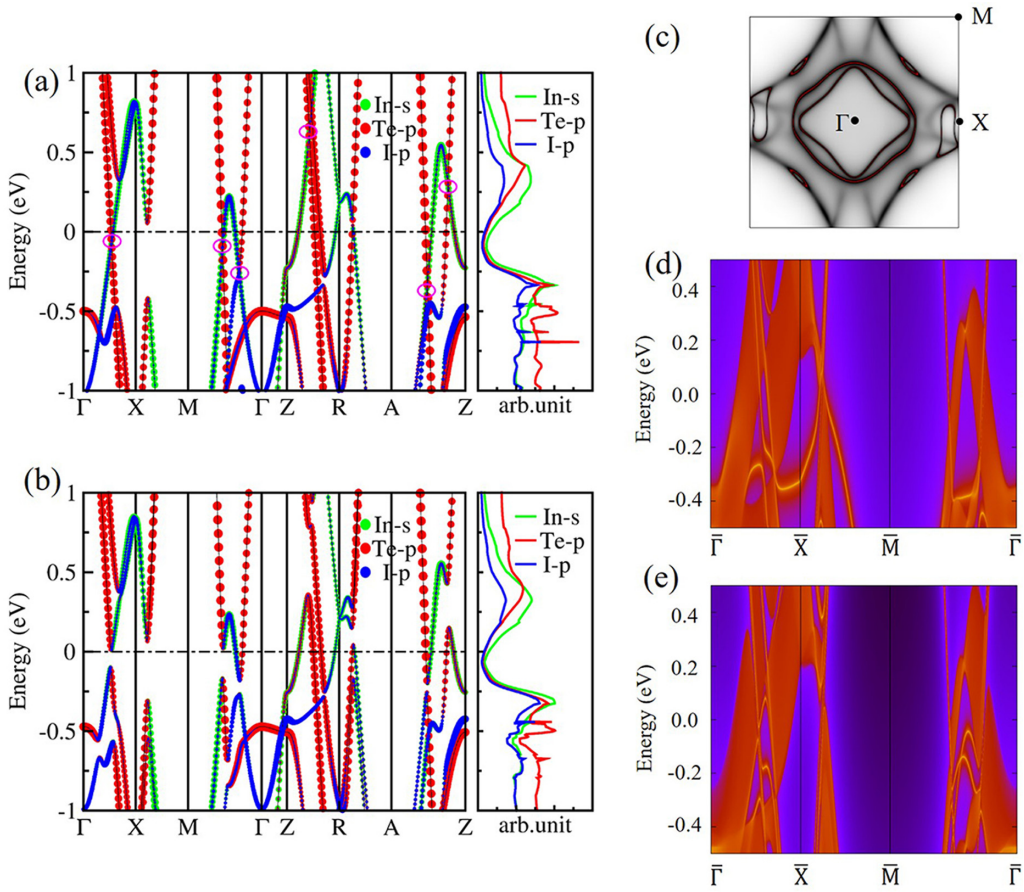

FIG. 6. The band structures of $P4/nmm$-II phase (a) without SOC show some band-crossing features can be identified as indicated by violet circles and (b) with SOC that the band inversion is mainly composed of the p orbital of Te atoms (red circles), I atoms (blue circles), and the s orbital of In atoms (green circles) in InTeI. (c) Projection of the diamond Fermi surface within the Γ–X–M plane. The projected surface density of states for the (100) surface (d) without SOC, and (e) with SOC.

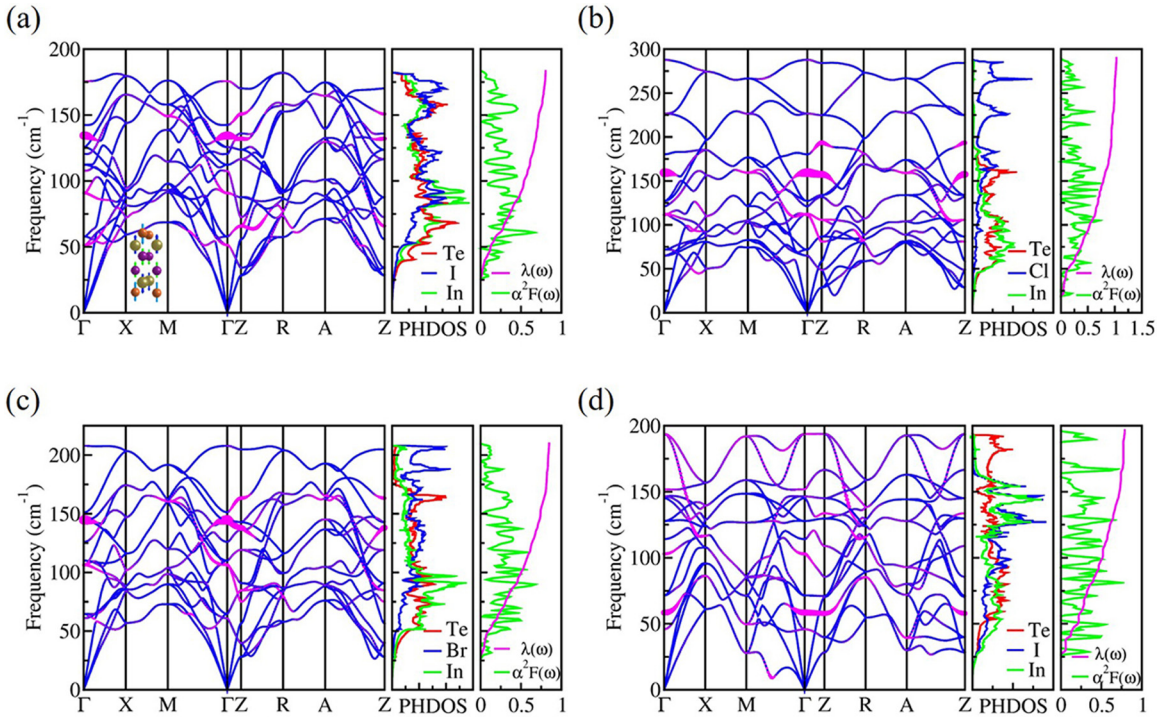

FIG. 7. Phonon dispersion curves, Eliashberg spectral functions $\alpha^2F(\omega)$ together with the electron-phonon integral $\lambda(\omega)$ and phonon density of states (PHDOS) for (a) $P4/nmm$-I of InTeI, (b) $P4/nmm$-I of InTeCl, (c) $P4/nmm$-I of InTeBr, and (d) $P4/nmm$-II of InTeI at 20 GPa, respectively. The phonon linewidth $\gamma_{q,j}(\omega)$ of each mode (q, j) is illustrated by the size of purple circles along with the phonon dispersions.

resulting in a continuous "band gap," even if several bands are crossing the Fermi level. Since the electronic structures are fully gapped, we have calculated the so-called Z_2 topological invariant through the evolution of hybrid Wannier center (0 or 1, indicating trivial or nontrivial topology, respectively). Our calculations reveal that the Z_2 comes out to be 1. This clearly indicates that the gapped state is topologically nontrivial.

To thoroughly testify the conclusion of topological semimetal, we next show the surface band structures on the (001) surface without and with SOC, presented in Figs. 6(d) and 6(e): InTeI has several nontrivial surface states, thereby in the presence of SOC this phase can be considered as a material similar to a topological insulator.

VI. PRESSURE-INDUCED SUPERCONDUCTIVITY

Motivated by the presence of metallic electronic band structure, it is reasonable to speculate that InTeI holds a good expectance to be a superconductor. In order to explore the superconducting characteristics of $P4/nmm$-I phase under pressure, the e-ph coupling constant λ was calculated. The Allen-Dynes modified McMillan formula [46,47],

$$T_C = \frac{\omega_{\log}}{1.2}\exp\left[-\frac{1.04(1+\lambda)}{(\lambda-\mu^*(1+0.62\lambda))}\right],$$

was used to estimate the T_c, with choosing the Coulomb pseudopotential $\mu^* = 0.1$. The logarithmically averaged phonon frequencies $\omega_{\log}$, and frequency-dependent e-ph coupling

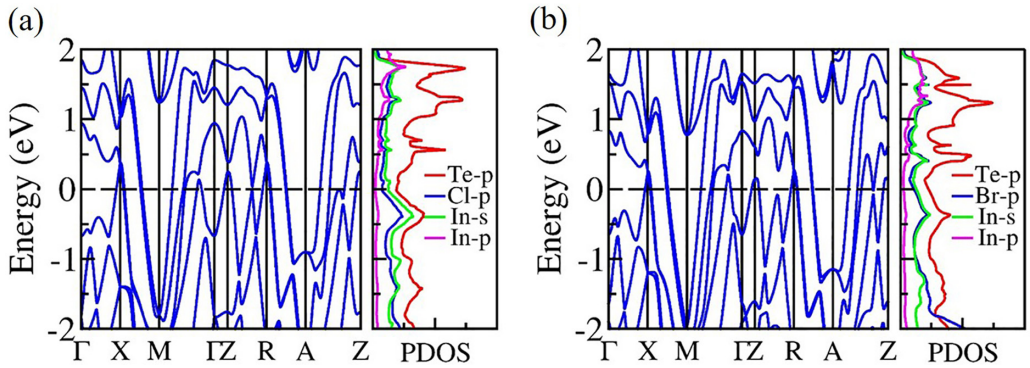

FIG. 8. Calculated electronic band structures and projected density of states for the $P4/nmm$-I structure of (a) InTeCl and (b) InTeBr at 20 GPa with SOC, respectively.

TABLE III. The *e*-ph parameter (λ), logarithmic average of phonon frequencies ($\omega_{\log}$), and estimated superconducting critical temperature (T_c) with the Coulomb potential (μ^*) of 0.1 for $P4/nmm$-I of InTeI, InTeBr, and InTeCl under 20 GPa.

Phase (pressure)	λ	$\omega_{\log}$ (cm^{-1})	T_c (K)
$P4/nmm$-InTeI (20 GPa)	0.81	114.5	5.4
$P4/nmm$-InTeBr (20 GPa)	0.85	125.8	6.6
$P4/nmm$-InTeCl (20 GPa)	1.03	133.8	9.7

$\lambda(\omega)$ can result from the Eliashberg spectral function $\alpha^2F(\omega)$. As Fig. 7(a) implies, the low-frequency vibrations extended to about $80\,\mathrm{cm}^{-1}$ are related to the vibrations of the Te and In atoms. Unlike the $P4/nmm$-I [Fig. 7(d)], the middle-frequency region of $P4/nmm$-II is associated with the I and In atoms, and the high-frequency modes come from the vibrations of the Te atoms. The predicted value of λ for the $P4/nmm$-I phase is 0.81, yielding high-pressure induced superconductivity with $T_c = 5.4$ K at 20 GPa. For the $P4/nmm$-II phase, the maximal λ equals 0.79, and T_c is about 5.2 K at 20 GPa. As the pressure increases, T_c of $P4/nmm$-I phase decreases.

The attempt to induce or enhance superconductivity properties of materials by atomic substitution in experiments results in a preferable outcome. We try to raise the T_c in $P4/nmm$-I structure by replacing the iodine atom with other lighter halogen atoms. In our calculations, the $P4/nmm$-InTeBr and $P4/nmm$-InTeCl are both metallic and stable at 20 GPa, as shown in Figs. 7 and 8. Our calculations reveal that both the $P4/nmm$-InTeBr and $P4/nmm$-InTeCl could be superconducting and with critical temperatures of 6.6 and 9.7 K at 20 GPa, respectively. The λ, $\omega_{\log}$, and T_c results for $P4/nmm$-InTeI, $P4/nmm$-InTeBr, and $P4/nmm$-InTeCl are collected in Table III.

As can be seen in Fig. 7, for $P4/nmm$-I of InTeI, InTeBr, and InTeCl, low-frequency phonon modes below $80\,\mathrm{cm}^{-1}$ give a contribution of 48.8, 40.7, and 39.2% to the *e*-ph coupling parameter λ at 20 GPa, respectively. In these phonon band structures, there are notable Raman active modes A_{1g} with dominant contributions to the *e*-ph coupling at the Γ point, depicted in Fig. 7(a): the vibrations of all atoms are perpendicular to the *ab* plane. Interestingly, the transverse acoustic (TA) modes of $P4/nmm$-InTeCl and $P4/nmm$-InTeBr along $Z \rightarrow R$ are softened under pressure. However the relatively small phonon linewidth of these modes indicates that they do not contribute much to the *e*-ph coupling.

Finally, based on the above discussions, we proposed the complex *P-T* phases diagram for InTeI, as shown in Fig. 9. As one can see in the literature, three kinds of phase transitions—structural phase transition, direct to indirect band-gap transition, and an insulator to metal transition with the emergence of superconductivity—contact each other. To explicitly explain these phase diagrams, further experiment observations under high pressure are desirable.

VII. CONCLUSIONS

In summary, using a machine-learning and graph theory accelerated crystal structure search package called MAGUS, we have investigated the pressure-induced phase transitions of InTeI. It is found that InTeI may undergo a transition from the ambient phase ($P2_1/c$) into a tetragonal phase $P4/nmm$-I, characterized by the insulator to metal transition. For the $P2_1/c$ phase, our calculations indicate a direct-indirect transition of band structure under the application of pressure. The metastable $P4/nmm$-II phase of InTeI is a possible topological metal with a band inversion along the $\Gamma \rightarrow M$ direction and a single Dirac cone at the $\bar{X}$ point when the SOC effect is included. We predict the superconducting transition temperature T_c of InTeI. The T_c of InTeI shows a slight tendency to decrease with the increasing pressure, but the superconducting state remains up to 40 GPa, the highest pressure we studied. By substituting iodine atoms in the $P4/nmm$-I phase with bromine and chlorine atoms, the T_c has a clear tendency to increase. These findings make this family of vdW-layered metal tellurohalides an excellent platform for the study of optoelectronic applications, and we hope this will stimulate experimental efforts to realize them in the laboratory.

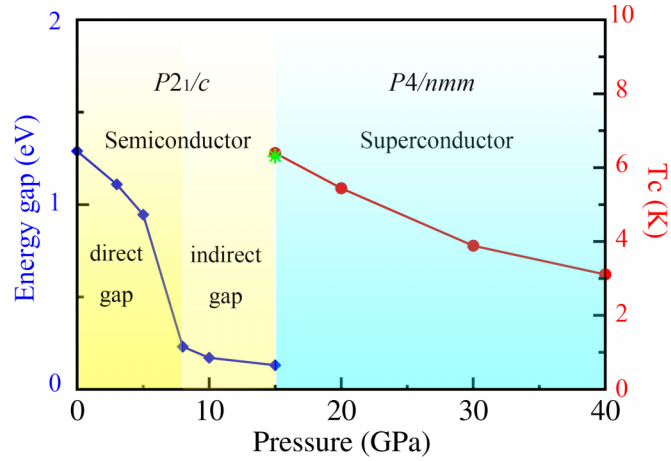

FIG. 9. Temperature-pressure phase diagram of InTeI, where blue diamonds represent the pressure dependence of the energy band gap, the red circles represent the pressure dependence of superconducting transition temperatures T_c of $P4/nmm$-I phase, and the green star represents T_c of $P4/nmm$-II phase at 20 GPa.

ACKNOWLEDGMENTS

J.S. gratefully acknowledges the financial support from the National Key R&D Program of China (Grant No. 2016YFA0300404), the National Natural Science Foundation of China (Grants No. 11974162 and No. 11834006), and the Fundamental Research Funds for the Central Universities. The calculations were performed using supercomputers at the High Performance Computing Center of Collaborative Innovation Center of Advanced Microstructures, the high-performance supercomputing center of Nanjing University, and "Tianhe-2" at NSCC-Guangzhou.

[1] K. Ishizaka, M. S. Bahramy, H. Murakawa, M. Sakano, T. Shimojima, T. Sonobe, K. Koizumi, S. Shin, H. Miyahara, A. Kimura *et al.*, Nat. Mater. **10**, 521 (2011).

[2] M. S. Bahramy, B. J. Yang, R. Arita, and N. Nagaosa, Nat. Commun. **3**, 679 (2012).

[3] X. Xi, C. Ma, Z. Liu, Z. Chen, W. Ku, H. Berger, C. Martin, D. B. Tanner, and G. L. Carr, Phys. Rev. Lett. **111**, 155701 (2013).

[4] M. K. Tran, J. Levallois, P. Lerch, J. Teyssier, A. B. Kuzmenko, G. Autes, O. V. Yazyev, A. Ubaldini *et al.*, Phys. Rev. Lett. **112**, 047402 (2014).

[5] Y. Chen, X. Xi, W.-L. Yim, F. Peng, Y. Wang, H. Wang, Y. Ma, G. Liu *et al.*, J. Phys. Chem. C **117**, 25677 (2013).

[6] I. P. Rusinov, T. V. Menshchikova, I. Y. Sklyadneva, R. Heid, K. P. Bohnen, and E. V. Chulkov, New J. Phys. **18**, 113003 (2016).

[7] Y. Qi, W. Shi, P. G. Naumov, N. Kumar, R. Sankar, W. Schnelle, C. Shekhar, F. C. Chou *et al.*, Adv. Mater. **29**, 1605965 (2017).

[8] S. Güler-Kılıç and Ç. Kılıç, Phys. Rev. B **91**, 245204 (2015).

[9] Q. H. Wang, K. Kalantar-Zadeh, A. Kis, J. N. Coleman, and M. S. Strano, Nat. Nanotechnol. **7**, 699 (2012).

[10] L. Fu, Y. Wan, N. Tang, Y.-m. Ding, J. Gao, J. Yu, H. Guan, K. Zhang *et al.*, Sci. Adv. **3**, e1700162 (2017).

[11] Y. Zhou, J. Wu, W. Ning, N. Li, Y. Du, X. Chen, R. Zhang, Z. Chi, X. Wang, X. Zhu *et al.*, Proc. Natl. Acad. Sci. USA **113**, 2904 (2016).

[12] K. Kirshenbaum, P. S. Syers, A. P. Hope, N. P. Butch, J. R. Jeffries, S. T. Weir, J. J. Hamlin, M. B. Maple *et al.*, Phys. Rev. Lett. **111**, 087001 (2013).

[13] C. Zhang, L. Sun, Z. Chen, X. Zhou, Q. Wu, W. Yi, J. Guo, X. Dong, and Z. Zhao, Phys. Rev. B **83**, 140504(R) (2011).

[14] J. L. Zhang, S. J. Zhang, H. M. Weng, W. Zhang, L. X. Yang, Q. Q. Liu, S. M. Feng, X. C. Wang, R. C. Yu, L. Z. Cao *et al.*, Proc. Natl. Acad. Sci. USA **108**, 24 (2011).

[15] X. Chen, P. Lu, X. Wang, Y. Zhou, C. An, Y. Zhou, C. Xian, H. Gao, Z. Guo, C. Park *et al.*, Phys. Rev. B **96**, 165123 (2017).

[16] A. Jain, S. P. Ong, G. Hautier, W. Chen, W. D. Richards, S. Dacek, S. Cholia, D. Gunter, D. Skinner *et al.*, APL Mater. **1**, 011002 (2013).

[17] G. Sawitzki, D. Müller, and H. Hahn, Mater. Res. Bull. **15**, 753 (1980).

[18] S. Jiang, J. Li, W. Chen, H. Yin, G. P. Zheng, and Y. Wang, Nanoscale **12**, 5888 (2020).

[19] X. Wang, J. Wu, J. Wang, T. Chen, H. Gao, P. Lu, Q. Chen, C. Ding, J. Wen, and J. Sun, Phys. Rev. B **98**, 174112 (2018).

[20] S. A. Kimber, A. Kreyssig, Y. Z. Zhang, H. O. Jeschke, R. Valenti, F. Yokaichiya, E. Colombier, J. Yan *et al.*, Nat. Mater. **8**, 471 (2009).

[21] M. Rotter, M. Tegel, and D. Johrendt, Phys. Rev. Lett. **101**, 107006 (2008).

[22] H. Takahashi, K. Igawa, K. Arii, Y. Kamihara, M. Hirano, and H. Hosono, Nature (London) **453**, 376 (2008).

[23] Q. Gu, P. Lu, K. Xia, J. Sun, and D. Xing, Phys. Rev. B **96**, 064517 (2017).

[24] K. Xia, H. Gao, C. Liu, J. Yuan, J. Sun, H.-T. Wang, and D. Xing, Sci. Bull. **63**, 817 (2018).

[25] C. Liu, J. Shi, H. Gao, J. Wang, Y. Han, X. Lu, H.-T. Wang, D. Xing, and J. Sun, Phys. Rev. Lett. **126**, 035701 (2021).

[26] B. Shahriari, K. Swersky, Z. Wang, R. P. Adams, and N. de Freitas, Proc. IEEE **104**, 148 (2016).

[27] C. Liu, H. Gao, Y. Wang, R. J. Needs, C. J. Pickard, J. Sun, H.-T. Wang, and D. Xing, Nat. Phys. **15**, 1065 (2019).

[28] Q. Gu, D. Xing, and J. Sun, Chin. Rev. Lett. **36**, 097401 (2019).

[29] P. E. Blochl, Phys. Rev. B **50**, 17953 (1994).

[30] G. Kresse and J. Furthmuller, Comput. Mater. Sci. **6**, 15 (1996).

[31] J. P. Perdew, K. Burke, and M. Ernzerhof, Phys. Rev. Lett. **77**, 3865 (1996).

[32] S. Grimme, J. Antony, S. Ehrlich, and H. Krieg, J. Chem. Phys. **132**, 154104 (2010).

[33] S. Grimme, S. Ehrlich, and L. Goerigk, J. Comput. Chem. **32**, 1456 (2011).

[34] J. Paier, M. Marsman, K. Hummer, G. Kresse, I. C. Gerber, and J. G. Angyan, J. Chem. Phys. **124**, 154709 (2006).

[35] A. Togo, F. Oba, and I. Tanaka, Phys. Rev. B **78**, 134106 (2008).

[36] A. A. Mostofi, J. R. Yates, Y.-S. Lee, I. Souza, D. Vanderbilt, and N. Marzari, Comput. Phys. Commun. **178**, 685 (2008).

[37] M. P. L. Sancho, J. M. L. Sancho, and J. Rubio, J. Phys. F **15**, 851 (1985).

[38] Q. Wu, S. Zhang, H.-F. Song, M. Troyer, and A. A. Soluyanov, Comput. Phys. Commun. **224**, 405 (2018).

[39] P. Giannozzi, S. Baroni, N. Bonini, M. Calandra, R. Car, C. Cavazzoni, D. Ceresoli, G. L. Chiarotti, M. Cococcioni, I. Dabo *et al.*, J. Phys.: Condens. Matter. **21**, 395502 (2009).

[40] J. Klimeš, D. R. Bowler, and A. Michaelides, Phys. Rev. B **83**, 195131 (2011).

[41] M. Dion, H. Rydberg, E. Schroder, D. C. Langreth, and B. I. Lundqvist, Phys. Rev. Lett. **92**, 246401 (2004).

[42] K. Lee, É. D. Murray, L. Kong, B. I. Lundqvist, and D. C. Langreth, Phys. Rev. B **82**, 081101(R) (2010).

[43] J. Klimes, D. R. Bowler, and A. Michaelides, J. Phys.: Condens. Matter. **22**, 022201 (2010).

[44] L. M. Schoop, M. N. Ali, C. Strasser, A. Topp, A. Varykhalov, D. Marchenko, V. Duppel, S. S. Parkin *et al.*, Nat. Commun. **7**, 11696 (2016).

[45] S. M. Young and C. L. Kane, Phys. Rev. Lett. **115**, 126803 (2015).

[46] P. B. Allen and R. C. Dynes, Phys. Rev. B **12**, 905 (1975).

[47] W. L. McMillan, Phys. Rev. **167**, 331 (1968).